

# 1 **Influence of the GDL and assembly mode of a PEM cell on the** 2 **ethanol revalorization into chemicals**

3 A. Rodríguez-Gómez, F. Dorado, A. de Lucas-Consuegra, A.R. de la Osa\*.

4 *Chemical Engineering Department, Faculty of Chemical Sciences and Technology,*  
5 *University of Castilla-La Mancha, Avda. Camilo José Cela 12, 13071, Ciudad Real,*  
6 *Spain. \*AnaRaquel.Osa@uclm.es*

## 7 **Abstract**

8 This work reports the influence of the gas diffusion layer (GDL) and cell assembly mode  
9 on the ethanol revalorization through the electro-reforming process, focusing on  
10 hydrogen and value-added organics (acetaldehyde, ethyl acetate and acetic acid) products  
11 distribution. All essays were conducted in a Proton Exchange Membrane (PEM)  
12 Electrolysis Cell of 5 cm<sup>2</sup> at mild conditions (80 °C and 1 atm) on commercial Pt/C  
13 (cathode) and PtRu/C (anode) catalysts. In this scenario the selection of a proper GDL  
14 and way of assembly proves to be a critical step influencing the electrochemical  
15 performance. Carbon paper-based configurations exhibited the best profiles in terms of  
16 electro-catalytic activity, reaching high current density values (600-720 mA·cm<sup>-2</sup> at 1.4  
17 V of cell potential), which are close to those obtained in alkaline media. Conversely, that  
18 based on porous titanium showed a lower efficiency (less than a half) due to the mass  
19 transfer limitations of reactants and products through the GDL, as confirmed by the  
20 electrochemical impedance spectroscopy essays. Regarding organic product distribution,  
21 non-assembled carbon paper-based configuration displayed the best results, increasing  
22 the production of value-added organics and shifting the acetic acid generation to lower  
23 cell potential values (close to 0.7 V). This was attributed to the direct deposition of the  
24 catalytic layers over the membrane instead of over the carbon GDL, which enhances the

1 reactants and ions transport, improving the electrochemical activity. In addition, this  
2 configuration showed quite lower energy requirements for H<sub>2</sub> production (<20  
3 kWh·kgH<sub>2</sub><sup>-1</sup> at 0.8 V) in comparison with a PEM water electrolyzer stack.

4 **Keywords:** Ethanol electro-reforming; PEM cell architecture; GDL; assembly mode;  
5 hydrogen; value-added organic production.

6

## 7 **1. Introduction**

8 The world total population has not stopped to increase since the middle of the 20<sup>th</sup> century  
9 which has caused a serious raise in the energy consumption. This fact, joined with the  
10 exhaustion of fossil fuels reserves, has led the scientific community the challenge of  
11 searching new and cleaner alternative ways of energy [1-3]. In this context, bioethanol  
12 has attracted great interest as fuel, due to its numerous advantages: it is nontoxic, safe,  
13 easy to transport (liquid compound) and has a higher energy density (8 kWh·kg<sup>-1</sup>) than  
14 other compounds such as methanol [4]. Also, it can be produced from biomass feedstock  
15 (energy crops, grain, corn...) becoming a renewable fuel as the total balance of carbon  
16 remains constant. It is widely used in gasoline (mainly in USA), and can be used more  
17 efficiently in fuel cells (DEFC), being one of the best substitutes to the internal  
18 combustion engines due to its low emission of pollutants [5]. Alternatively, bioethanol  
19 can be electro-oxidized in a proton exchange membrane (PEM) ethanol electrolysis cell  
20 (EEC) to produce hydrogen, which is considered an interesting energy vector in the last  
21 decades [6]. The viability of hydrogen generation from light alcohols is well developed  
22 in the current literature [7-13], requiring lower energy consumption (25-30 kWh·kgH<sub>2</sub><sup>-1</sup>)  
23 than water electro-reforming systems (50 kWh·kgH<sub>2</sub><sup>-1</sup>), which constitutes an attractive  
24 process from an industrial point of view [14]. In an EEC, ethanol is electro-oxidized at

1 the anodic side of a PEM cell, leading to the formation of carbon dioxide, protons and  
2 electrons (Eq. S1 from the supplementary information (SI),  $n = 12$  transferred electrons).  
3 The external circuit provides the electrical potential to drive the reaction, while protons  
4 migrate through the proton exchange membrane to the cathode side, where they  
5 recombine with electrons generating high purity hydrogen (Eq. S2). However, in the  
6 practice, low yields towards CO<sub>2</sub> have been **generally** reported due to the high energy  
7 requirements to break the C-C bond. This results in a partial ethanol electro-oxidation  
8 with the formation of different organic compounds such as acetaldehyde (Eq. S3-S5), and  
9 in a less concentration, acetic acid (Ec. S6-S8) [15]. In this scenario, different authors  
10 have focused on the study of anodic electro-catalysts with the purpose of improving the  
11 reaction kinetic of ethanol oxidation. Thus, bimetallic catalysts such as Pt-Ru/C and Pt-  
12 Sn/C, among others, have proved to be a suitable option promoting the electrochemical  
13 process [16-21]. However, this is not the only important parameter to consider of this  
14 technology since the cell architecture could play a key role in the electro-reforming  
15 process. In general terms, a typical PEM cell unit includes a membrane electrode  
16 assembly (MEA) sandwiched between the flow field plates (FFPs) of the anode and  
17 cathode, into which flow channels are grooved. The MEA is the most important part of  
18 the cell, containing two gas diffusion and catalyst layers (GDLs and CLs) on the anode  
19 and cathode side respectively, and a proton exchange membrane in between [22]. The  
20 GDL plays a very important role in the performance of these devices, allowing an efficient  
21 transfer of the reactants to the catalytic layer and a correct evacuation of the produced  
22 compounds. Also the mass transport in the diffusion layer seems to have a strong effect  
23 on the PEM cell behaviour, being able to decrease the efficiency of the process [23].  
24 Parameters such as thickness and porosity of the layers, permeability, or conductivity,  
25 along with suitable compression conditions and reaction area position in the catalyst

1 layers must be considered [24-28]. In this context, different authors have studied the GDL  
2 type and MEA architecture testing different materials [22, 23, 29-33] and modifying the  
3 pressure conditions of MEA assembly [34]. However, these studies deal with the  
4 management of generated water in the cathode side of a PEMFCs in order to avoid the  
5 flooding or dehydration processes [35], limiting the mass transport of oxygen to the  
6 catalyst. In this sense, most of the available current literature is related to the fuel cells  
7 field, while papers which deal with the influence of the MEA architectures on the alcohol  
8 electro-reforming performance are scarce [36]. Therefore, in order to reach a compromise  
9 between both performance for alcohol electro-reforming and cost requirements, the  
10 structural, electrochemical and transport parameters that characterize the GDL and  
11 assembly conditions in the PEM cell need to be optimized.

12 Other point to highlight is the product distribution obtained from ethanol electro-  
13 oxidation. Most of the authors have exclusively focused on the hydrogen production rates  
14 on the cathode. However, the anodic co-production of value-added organics such as  
15 acetaldehyde, acetic acid or ethyl acetate would be more advantageous from an  
16 economical point of view. Therefore, the overall obtained profit of the process could be  
17 increased from the simultaneous production of all those compounds, mainly if the  
18 selectivity toward acetic acid is high. In this sense, the electro-catalytic pathway is  
19 presented as a promising alternative to the traditional systems, since it is possible to  
20 simultaneously co-produce hydrogen and value-added organic compounds in an only  
21 reaction step, directly separated into two compartments (anode and cathode chambers).  
22 Furthermore, the use of a PEM cell reactor brings several advantages such as potential  
23 energy savings and reduction of the environmental impact, compared with those coming  
24 from the acetaldehyde (Wacker process) [37], hydrogen (natural gas steam reforming)  
25 and acetic acid (methanol carbonylation) conventional production processes. In addition,

1 it is a compact device easily to scale by modulation and it is possible to couple with  
2 renewable energy systems.

3 Taking all into account, the aim and contribution of the present work is to evaluate the  
4 influence of different MEA architectures (varying the GDL type, catalyst layer support  
5 and way of assembly) on the ethanol electro-reforming process, focusing on the product  
6 distribution (hydrogen and organic compounds) in order to accomplish a better ethanol  
7 revalorization.

## 8 **2. Material and methods**

### 9 **2.1 Membrane electrode assembly (MEA) preparation using different configuration**

10 In this paper three configurations of membrane electrode assembly (MEA) named *a*, *b*  
11 and *c* were tested in order to study the influence of the gas diffusion layer (GDL) and  
12 assembly mode on the ethanol electro-oxidation, focusing not only on the activity but also  
13 on the product distribution.

14 Bimetallic commercial catalysts of Pt-Ru (Ru-40% Pt-20% PtRu/C-Alfa Aesar) and Pt  
15 supported on carbon (20% Pt/C-Alfa Aesar) were used as the anode and cathode,  
16 respectively, and for all configurations. Coating inks containing proper amounts of each  
17 electrocatalyst were prepared to obtain a loading of 1.5 mg/cm<sup>2</sup> for the anode and 0.5  
18 mg/cm<sup>2</sup> for the cathode electrode. To this purpose, catalysts in powder form were  
19 dispersed in a solution of Nafion ionomer (5 wt. %, Sigma- Aldrich) and 2-propanol with  
20 a binder/catalyst weight ratio of 3.64. Then, ink solutions were sonicated for 2 h using an  
21 ultrasonic bath (110 W/50-60 Hz, Selecta) before deposition.

22 On the other hand, a proton conducting Nafion membrane of 180 μm thickness (supplied  
23 by Hydrogen Works) was used as the electrolyte. As described in other studies [9, 38],

1 prior to use, the polymeric membrane was pretreated through successive immersion in  
2 H<sub>2</sub>O<sub>2</sub> and H<sub>2</sub>SO<sub>4</sub> solutions (100 °C for 3 h) and finally in deionized water.

3 So-called configuration *a* corresponds to the conventional configuration used by many  
4 authors [39-41] and served as standard. It was formed by a GDL of carbon paper TGP-  
5 H90 (0.25 mm, supplied by Fuel Cells Earth), which also worked as a support for the  
6 metal active catalytic layer. Inks were thus deposited on carbon paper substrates by spray  
7 at 80 °C in order to evaporate the 2-propanol present in the solution, obtaining the metal  
8 loading specified above. Finally, different hot-pressing steps were conducted at different  
9 levels of temperatures from 30 °C to 120 °C at intervals of 10 °C. Each level was kept for  
10 1 min and in the last step 1 metric ton was applied for 3 min.

11 Configuration *b* uses two porous titanium plates (0.5 mm) as GDLs instead of carbon  
12 paper. In this case, inks deposition was carried out directly on both sides of the polymeric  
13 membrane, which worked as a support instead of the GDL. This resulted in a fine catalytic  
14 layer which could reduce ohmic resistance of the process (related to the mechanical part  
15 of the cell). Moreover, in this case, there was no need for a heating-pressure assembly  
16 step but the simply sandwich of the membrane (with the catalytic layer) and porous  
17 titanium plates with the rest of components of the cell in the montage step.

18 Finally, configuration *c* combines both previous configurations. This way, the GDL  
19 employed here was carbon paper (same specifications as for configuration *a*) and the  
20 deposition of the inks was carried out directly on the membrane sides (as for configuration  
21 *b*), avoiding the high-pressure assembly stage.

22 Figure 1 shows a scheme of the three proposed MEA configurations.

23

24

## 1 **2.2 Electrochemical reforming of ethanol in a proton exchange membrane reactor**

2 Experimental tests were carried out in a PEM electrolysis cell SQUAREPARK 5  
3 (purchased from Pragma Industries) with a geometric surface area of 5 cm<sup>2</sup>. The MEA  
4 was introduced between two Teflon gaskets designed to avoid short-circuiting of the cell.  
5 Graphitic bipolar plates of 5 mm thickness and 25 cm<sup>2</sup> of area were placed on both sides  
6 of the MEA. The plates present parallel indentations, with 1 mm x 1 mm of depth and a  
7 total volume of 3.51 cm<sup>3</sup>. Also these components count with a hole of 1.5 mm of diameter  
8 to introduce a thermocouple to control the temperature of the process. In order to ensure  
9 the sealing between anode and cathode compartments various o-ring were placed in the  
10 graphite plates. These latter are in contact with two gold-plated copper alloy electrical  
11 collectors, which allow the transmission of the electrical current to the graphite plates.  
12 Finally, all the above items were placed between two external compression plates of steel  
13 (16 mm of thickness and 64 cm<sup>2</sup> area) applying a par of 1 Nm with a torque wrench.

14 The anode compartment of the cell was supplied with a 4 M water/ethanol solution, while  
15 deionized water was fed to the cathode, in order to keep a suitable humidity on the  
16 membrane. Both streams were preheated at 80 °C and flow rates were regulated using a  
17 peristaltic multichannel pump (Heidolph 5001), fixing the value in 2 mL·min<sup>-1</sup> for the  
18 anode and cathode respectively, according to previous works [42]. The anodic chamber  
19 of the PEM reactor operated in continuous mode, while the deionized water was  
20 recirculated in the cathode. In addition, a cooling condensation column was installed (- 6  
21 °C) with the purpose of avoiding ethanol evaporation in the feeding reservoir.

22 Electrochemical measurements were carried out using a potentiostat/galvanostat  
23 VERTEX 5V (Ivium technology) controlled by a Research Electrochemistry software.  
24 Polarization curves were conducted at a potential range between 0-1.4 V and 20 mV·s<sup>-1</sup>  
25 scan rate in order to study the electro-catalytic performance related to each configuration.

1 Then, an electrochemical impedance spectroscopy essay (0.1-10000 Hz and 1 mV of  
2 amplitude) was carried out in the range of 0.5 to 0.9 V with the aim to determine the  
3 different resistances involved in the process. Moreover, chronopotentiometry essays were  
4 carried out to determine the as-derived product distribution (organic compounds and  
5 hydrogen). To that purpose, different levels of constant current, ranging from 0.2 to 0.8  
6 A at intervals of 0.2 A, were applied. Each level was kept for 500 s. The organic value-  
7 added liquid production was then analyzed offline (every 15 min), in an Agilent  
8 Technologies 8220A gas chromatograph equipped with a FID detector and a capillary  
9 column (Agilent DB-WAS UI, 30 m x 0.250 mm x 0.25  $\mu\text{m}$ ), using helium as a carrier  
10 gas. Hydrogen production flow rate from the cathodic compartment was measured by a  
11 high-precision flowmeter (supplied by Mervilab) and compared with the theoretical one  
12 via Faraday's Law. In order to check the stability of the system, a mild-term  
13 electrochemical reforming experiment was carried out for 2 h operating under 0.5 A  
14 constant current density ( $0.1 \text{ A}\cdot\text{cm}^{-2}$ ). Finally, for configuration *b*, this technique was also  
15 conducted applying OCV cycles of 30 s every 30 min.

### 16 **3. Results and discussion**

17 In order to study the electro-catalytic performance for the three proposed configurations,  
18 a linear sweep voltammetry test was performed. First, the applied potential was verified  
19 to be invested in the alcohol electro-reforming process excluding water electrolysis  
20 contribution. For that purpose, a separate experiment with only deionized water was  
21 conducted at 80 °C and room pressure screening a potential range between 0 to 2.5 V at  
22  $20 \text{ mV}\cdot\text{s}^{-1}$  of scan rate. Figure 1S from the SI (supplementary information) shows the  
23 comparison between these results with the profile obtained for 4 M ethanol/water mixture  
24 recorded at the same conditions (within an interval of 0-1.4 V) using the configuration *a*.  
25 Note that hydrogen production is only attributed to the alcohol electro-oxidation, since

1 no current density was obtained at this potential range (0-1.4 V) with the deionized water  
2 experiment, checking the onset potential for water electrolysis close to 1.4 V. After  
3 proving the viability of the system, a comparative study among the different  
4 configurations was accomplished. Figure 2 depicts the comparative between the linear  
5 sweeps for the three configurations at  $2 \text{ ml}\cdot\text{min}^{-1}$ ,  $80 \text{ }^\circ\text{C}$ , room pressure and 4 M  
6 ethanol/water solution. In general terms, a typical trend was obtained: current density and  
7 hence hydrogen production rate increased as along with the applied potential, which is  
8 attributed to the enhanced kinetic of the electrochemical reaction by increasing the driving  
9 force. At low polarization levels the process is governed by kinetic limitations, showing  
10 the onset potential for ethanol electro-reforming close to 0.4 V (although partial ethanol  
11 electro-reforming is thermodynamically favoured at a potential higher 0.08 V [43]). In  
12 this sense, non-important activity toward  $\text{H}_2$  and organic liquids was observed for this  
13 potential range, since no current density was registered. This suggest that in this potential  
14 range there are some kinetic limitations (activation energy,) requiring an increase in the  
15 driving strength and consequently, a rise in the overpotential. At an intermediate potential  
16 range (0.5-1 V), the system follows an ohmic behaviour being able to adjust to a straight  
17 line. It can be observed that the slopes for both carbon paper configurations (*a* and *c*) were  
18 considerably higher than that obtained for configuration *b*, using porous titanium as GDL,  
19 which showed lower values of current density. Finally, at high polarization levels, the  
20 system starts to be limited by the mass transfer resistance, especially when the electro-  
21 catalytic activity is high, reaching a final current density of  $600 \text{ mA}\cdot\text{cm}^{-2}$ ,  $250 \text{ mA}\cdot\text{cm}^{-2}$   
22 and  $725 \text{ mA}\cdot\text{cm}^{-2}$  for configurations *a*, *b* and *c* respectively at 1.4 V. Accordingly, the  
23 worst result in terms of electro-catalytic activity was obtained for configuration *b*, where  
24 mass transfer limitations seemed to take place at lower potentials values (from 0.8 V) than  
25 those for configurations *a* and *c*, preventing from a proper electro-catalytic performance.

1 This fact can be attributed to the properties and characteristics of the material employed  
2 as a GDL. The porous titanium thickness is twice that of carbon paper, which could derive  
3 in a higher resistance to mass transfer for reactants and products involved in the  
4 electrochemical reactions, and even for the ions transported through the GDL. It can be  
5 also observed that between the two configurations which used carbon paper as a GDL,  
6 configuration *c* is highlighted. Note that a maximum current density of  $720 \text{ mA}\cdot\text{cm}^{-2}$  was  
7 reached at the end of the explored interval, which is very promising compared with  
8 previous works on ethanol electro-reforming carried out under the same operation  
9 conditions ( $200 \text{ mA}\cdot\text{cm}^{-2}$  at 1.1 V, close to 4 times lower than that presented in this work)  
10 [9, 11] and very similar to those obtained in basic media (theoretically more efficient)  
11 [44]. For this configuration, the mass transfer resistance took place at the end of the  
12 potential range (from 1.3 V) compared to the configuration *a*, where the efficiency loss  
13 in the current density starts to be appreciable from 1 V of applied potential. This  
14 phenomenon could be explained attending to differences in the electrode preparation and  
15 the assembly mode of the MEA. In case of configuration *a*, inks deposition was carried  
16 out over the carbon paper requiring a high pressure-temperature assembly step to conform  
17 the MEA. However, for configuration *c*, inks were deposited directly on both sides of the  
18 membrane. This results in the formation of a more homogenous catalytic layer on the  
19 membrane surface, which could enhance the reactants and ions transport, shifting mass  
20 transfer limitations to higher potential values. Moreover, this configuration seemed to  
21 allow a better GDL-membrane contact without an assembly step, which would avoid  
22 possible damages in the GDL surface during the preparation (breakages, pore blockage).  
23 In order to better support the proposed hypothesis, electrochemical impedance  
24 spectroscopy essays were conducted. This technique allows quantifying the different  
25 resistances involved in the electro-reforming process. First, the influence of the potential

1 in the total resistance was evaluated for each configuration. Essays were performed at 80  
2 °C for 4 M of ethanol/water solution and  $2 \text{ ml} \cdot \text{min}^{-1}$  varying the cell potential from 0.5 to  
3 0.9 V. Also, the frequency range was fixed between 0.1-10000 Hz with 1 mV of  
4 amplitude. Experimental data were fitted to an equivalent electrical circuit formed by 3  
5 resistors ( $R1$ ,  $R2$  and  $R3$ ) and 2 capacitors ( $C1$  and  $C2$ ) as summarized in Table 1.  $R1$  is  
6 associated with the resistance of the MEA, while the sets  $R2-C1$  and  $R3-C2$  are associated  
7 with the anode and cathode resistances, respectively. Figure 3.a shows the Nyquist  
8 diagram for configuration *a* (rest of configuration are not shown since the behaviour is  
9 analogous). In general terms, an increase in the applied potential causes a decrease in the  
10 offered resistance toward the ethanol oxidation reaction, and hence an enhancement in  
11 the electro-catalytic activity due to a rise in the kinetics of the process. This decline in the  
12 resistance values are clearly visible at low potential range (0.5-0.7 V) where  $R2$  varies  
13 from 0.813 to 0.515 ohm and  $R3$  from 0.099 to 0.056 ohm. At higher potential range (0.7-  
14 0.9 V), the differences start to be lower reaching very similar resistance values (see Table  
15 1). This fact is attributed to the mass transfer limitations that take place at high potential  
16 levels (as corroborated in the LSV tests, Figure 2), which correspond to a maximum in  
17 the EOR kinetics, and therefore, to the obtention of minimum resistance values close to  
18 0.44 and 0.06 ohm for  $R2$  and  $R3$ , respectively. Note that  $R3$  value for the last potential  
19 step (0.9 V) is lightly increased from 0.056 to 0.062 ohm. Considering the experimental  
20 error in the mathematical fitting model process (up to 5%), these small differences would  
21 be within the limits of the standard deviation, and then, the last three cathodic resistances  
22 values ( $R3$ ) can be considered practically constant. Even with this, it is important to  
23 highlight that despite of this slight variation in the  $R3$  parameter, the total impedance  
24 value (sum of  $R1$ ,  $R2$  and  $R3$  contribution) decreases with the increase in the potential for  
25 the last interval of study (check the x-axis cutting point at 0.8-0.9 V, Figure 3.a). Also, it

1 can be observed that  $R1$  remains practically constant in the whole potential range, which  
2 proves that the MEA resistance is independent of the applied potential. Note that  $R2$   
3 values (anode) are always higher than  $R3$  values (cathode). Therefore, the rate  
4 determining step of the electro-reforming process seems to be caused by the anodic  
5 reaction (ethanol rupture) more than by protons and electrons recombination for hydrogen  
6 production in the cathodic chamber. Once the potential influence in the total impedance  
7 was accomplished, a comparative between the impedance values obtained for each  
8 configuration is showed in Figure 3.b at 0.5 V of cell potential. In general terms, porous  
9 titanium-based configuration exhibited the highest  $z''$ , which is reflected in the fitted  
10 parameters summarized in Table 2. It can be observed that all the architectures studied  
11 presented low  $R1$  values compared with the rest of parameters, being the MEA  
12 contribution negligible in the total cell impedance. Resistances associated with anode and  
13 cathode were considerably higher for porous titanium configuration compared with  
14 carbon paper-based ones. This effect can be sharply appreciated for  $R2$  parameter,  
15 reaching values of 3.41, 0.81 and 0.77 ohm for the configurations  $b$ ,  $a$  and  $c$  respectively.  
16 In this sense, porous titanium architecture offers a higher anodic and cathodic charge  
17 transfer resistance, limiting the transport for reactants and products through the GDL.  
18 This is in consonance with the results obtained in the linear sweeps voltammetry tests  
19 detailed above, where the configuration  $b$  exhibited the lowest electro-catalytic  
20 performance.  
21 However, small differences were found for the carbon paper configurations. Anyway, the  
22 anodic and cathodic resistances ( $R2$  and  $R3$ ) were slightly lower for configuration  $c$ ,  
23 which may improve the performance of the system. This corroborates the hypothesis  
24 proposed in this work, where the new membrane-electrode-assembly set formed by a

1 catalytic layer deposited directly over the membrane leads to an enhancement of mass  
2 transport, which increases the activity of the ethanol electro-reforming process.

3 Chronopotentiometry measurements were then carried out for a 4 M water/ethanol  
4 solution at 80 °C and different current steps (i.e. 0.2, 0.4, 0.6 and 0.8 A, which correspond  
5 to 40, 80, 120 and 160 mA·cm<sup>-2</sup> of current density, respectively) for 500 s. The purpose  
6 was to evaluate the product distribution (organic compounds and hydrogen) and energy  
7 requirements related to each level of applied current. Figure 4 shows the potential vs. time  
8 profile for each of the three configurations at four different applied current values. An  
9 increase in the potential with the current was registered for all architectures, as it  
10 corresponds to the behaviour of this type of systems. For the same current, the lowest  
11 potential values were attained with the carbon paper configurations (*a* and *c*), fact that  
12 significantly influences on the total cell energy consumption. In addition, these  
13 configurations showed a stable potential profile vs. time on stream for each current step,  
14 as a steady state was always reached at the beginning of each polarization. On the other  
15 hand, configuration *b* shows very unstable profiles mainly from the third applied current  
16 step (0.6 A, 120 mA·cm<sup>-2</sup>). At this level, a considerably increase in the potential was  
17 registered, exceeding the 1.4 V range, indicating that water and ethanol electro-reforming  
18 processes simultaneously occurred (as demonstrated in Figure 1S, SI). In this sense, the  
19 mass transfer limitations associated to the porous titanium GDL cause an increase in the  
20 driving force in order to keep the kinetics imposed at this level of applied current  
21 (demanded hydrogen production), shifting the potential to more positive values and  
22 consequence, reaching the water electrolysis region. [Note that despite of the mass transfer](#)  
23 [limitations take place from the third step of fixed current, the effect caused by the porous](#)  
24 [titanium GDL was also noticeable at low current levels \(0.2-0.4 A\). At this range, the](#)  
25 [potential values registered for configuration b \(0.62-0.8 V\) were higher than those](#)

1 obtained for the rest of layouts (close to 0.6-0.7 V). The porous titanium GDL presents a  
2 higher thickness and a lower porosity compared with carbon paper, which hinders the  
3 transport mechanism of the ions, offering a higher electrochemical resistance for the  
4 suitable development of the EOR process (as it was corroborated in the impedance essays,  
5 Figure 3). Therefore, in order to keep the kinetics imposed at this level of applied current  
6 the system reacts with an increase in the required cell potential. This would be in  
7 consonance with the LSV tests (Figure 2), where the electro-catalytic activity for  
8 configuration *b* was always lower than the rest for the whole range of study (0-1.4 V).

9 Regarding the total product generation, hydrogen production was measured and  
10 compared with the theoretical one expected. As an example, results for the configuration  
11 *a* are displayed in Figure S2 (SI). The rest of layouts presented an identical profile. Note  
12 that experimental hydrogen rates obtained for each applied current step are similar to  
13 those calculated via Faraday's law, confirming that there are not faradaic losses related  
14 to the hydrogen production. In addition, from experimental hydrogen flow rate data and  
15 the potential-current profile depicted in Figure 4, it was possible to calculate the  
16 corresponding energy requirements, expressed in  $\text{kWh}\cdot\text{kgH}_2^{-1}$ , for the three  
17 configurations at each current level. Note that an average potential ( $V_m$ ) was used in all  
18 calculations, since the steady-state regime was quickly reached, mainly for carbon paper  
19 configuration. All data were collected in Table 3. As expected, the required power (W)  
20 and total energy consumption ( $\text{kWh}\cdot\text{kgH}_2^{-1}$ ) increases proportionally to the applied  
21 current, as the proportion with that the required power increases is higher than the rise in  
22 the hydrogen flow rate production. The lowest energy requirements were obtained for  
23 configurations *a* and *c* ( $14\text{-}22 \text{ kWh}\cdot\text{kgH}_2^{-1}$  at  $40\text{-}160 \text{ mA}\cdot\text{cm}^{-2}$ ), which showed a quite  
24 similar profile. Configuration *b* exhibited higher potential ranges, demanding twice the  
25 power to produce the same amount of hydrogen, especially at the last two current steps,

1 where very high potential values (0.9 V to 1.8 V) were reached resulting in a consumption  
2 range comprised between 35.2-44.6 kWh·kgH<sub>2</sub><sup>-1</sup>. Note that these energy requirements are  
3 closer to the consumption of a PEM water stack (50 kWh·kgH<sub>2</sub><sup>-1</sup>) [9], as part of the total  
4 energy is being invested in the water electrolysis process, decreasing the cell energetic  
5 efficiency.

6 Along with H<sub>2</sub> production, in order to study the influence of the proposed configurations  
7 on the organic product distribution and, hence, the viability of ethanol valorization  
8 towards other value-added compounds, the anodic effluent was also analyzed. Figure 5  
9 shows the organic production flow rates obtained for each layout at the different current  
10 steps. It can be observed that, regardless of the configuration, the main anodic product  
11 was acetaldehyde, followed by ethyl acetate and acetic acid, whose production was  
12 strongly related to the cell potential. H. Li et al. [45] suggested that, under the application  
13 of low cell potentials, adsorption and dissociation of ethanol take place mainly on Pt sites,  
14 producing acetaldehyde (Eq. S3-S5, SI). The subsequent oxidation of this molecule would  
15 generate reaction intermediates (CH<sub>3</sub>CHO<sup>•</sup> species) which remain strongly chemisorbed  
16 on the Pt active sites, leading to the poisoning of the anodic catalyst, thus inhibiting the  
17 electro-reforming process. On the other hand, under the application of higher cell  
18 potentials, water molecules could be activated in order to produce active OH<sup>•</sup> species that  
19 are adsorbed on the Ru surface [45, 46] (Eq. S9, SI), which can further oxidize the  
20 adsorbed acetaldehyde leading to the formation of acetic acid (Eq. S6-S8, SI). Although  
21 in general the onset potential associated to each organic compounds obtained in this work  
22 are in consonance with those reported in the literature, the MEA architecture was found  
23 to modify the liquid product distribution, as explained below.

24 As expected, acetaldehyde was generated for the whole intensity range of study (0.2-0.8  
25 A) from 0.5 V steady-state cell potential, since according to the ethanol reaction

1 mechanism it is kinetically favored (0.082 V of theoretical potential). Carbon paper-based  
2 configurations (Figures 5.a and 5.c) exhibited similar ranges of acetaldehyde production,  
3 which were comprised between  $1.6 \cdot 10^{-3}$ - $6 \cdot 10^{-3}$  g·min<sup>-1</sup> and  $2.3 \cdot 10^{-3}$ - $6.3 \cdot 10^{-3}$  g·min<sup>-1</sup> for  
4 configurations *a* and *c*, respectively. Also, the overall production rate increases with the  
5 applied current, which corresponds with a higher level of cell potential and, therefore, a  
6 further progress in the electro-oxidation reaction mechanism. However, this trend was not  
7 fulfilled in configuration *b* (Figure 5.b), mainly from the third current step (0.6 A, 120  
8 mA·cm<sup>-2</sup>) to the end of the range. In this case, a decrease in the production rate was  
9 registered at higher cell potential values, which can be attributed to the simultaneous  
10 water electro-reforming process, as already commented above. In this sense, under these  
11 conditions, a competition between oxygen evolution and ethanol oxidation reactions  
12 seems to take place in the anodic compartment. Therefore, not all the applied energy is  
13 invested in the alcohol electro-reforming process and much of the total hydrogen is  
14 produced from water electrolysis, causing efficiency losses in terms of organic  
15 compounds generation.

16 Ethyl acetate begins to be produced from the second current level (0.4 A, 80 mA·cm<sup>-2</sup>) at  
17 cell potential values close to 0.6 V (for the three configurations) but it is generated in a  
18 much smaller proportion than acetaldehyde ( $1.7 \cdot 10^{-4}$  -  $5.6 \cdot 10^{-4}$  g·min<sup>-1</sup>), being around 8  
19 wt. % of the total organic liquid production.

20 Acetic acid production occurred at different potentials levels depending on the  
21 configuration being tested. Thus, configuration *a* exhibited a low acetic acid production  
22 close to  $1.22 \cdot 10^{-4}$  g·min<sup>-1</sup>, which only occurred from the last current step at 0.8 V.  
23 However, configuration *c* seemed to enhance the generation of this compound since its  
24 production is shifted to a lower cell potential (0.7 V) from the second current step. Also,  
25 the range of production associated with configuration *c* was higher, approximately four

1 times ( $1.3 \cdot 10^{-4}$ - $4 \cdot 10^{-4}$  g·min<sup>-1</sup>) than that obtained by configuration *a*. This is attributed to  
2 the morphology and thickness of the catalytic layer depending on the material used as  
3 support. Therefore, the direct deposition of both electrodes over the membrane surface  
4 appeared to enhance the transport mechanism, increasing not only the electro-catalytic  
5 activity but also the selectivity toward acetic acid. On the other hand, despite of the mass  
6 resistance limitations offered by configuration *b* (demonstrated in the impedance study,  
7 Figure 3), porous titanium architecture exhibited an acetic acid production slightly higher  
8 ( $2 \cdot 10^{-4}$ - $5 \cdot 10^{-4}$  g·min<sup>-1</sup>) than that of configuration *c*. However, note that the potential range  
9 was considerably higher for this configuration (0.8-1.66 V) obtaining consumption values  
10 per kg of acetic acid close to 44 kWh·kgC<sub>2</sub>O<sub>2</sub>H<sub>4</sub><sup>-1</sup>, a low competitive result compared to  
11 that obtained for configuration *c* (26 kWh·kgC<sub>2</sub>O<sub>2</sub>H<sub>4</sub><sup>-1</sup>).

12 Furthermore, it is important to mention that the formation of other reaction products such  
13 CO<sub>2</sub> was not detected. This compound is strongly limited in these systems, as the Pt-Ru  
14 has a poor activity toward the scission of C-C bonds under low temperature conditions  
15 (temperatures below 100 °C). In order to check the possible generation of this compound  
16 a chronopotentiometry was carried out at 0.5 A for 3 h (not shown in this study), where  
17 approximately less than 1% in mole fraction of CO<sub>2</sub> was obtained working even in recycle  
18 mode of operation.

19 Once studied the ethanol electro-reforming to different value-added ethanol-derived  
20 compounds, and with the purpose of demonstrating the stability of each configuration for  
21 future practical applications, a mild-term galvanostatic essay was conducted at 0.5 A (100  
22 mA·cm<sup>-2</sup>) and 80 °C for 2 h by feeding a 4 M water/ethanol solution (2 ml·min<sup>-1</sup>). The  
23 selection of this applied current level was due to comparative purposes with the existing  
24 data from the literature. Different authors have studied the stability of the EOR process  
25 at these current values (0.5 A, 100 mA·cm<sup>-2</sup>) in both electrolysis [9, 11, 47, 48] and fuel

1 cell modes [49]. In this sense, to run this essay at the same operating conditions is  
2 essential to avoid errors in the comparison of system efficiencies since the consumption  
3 values hardly depends on the applied current. Figure 6.a depicts the variation of the cell  
4 potential with time on stream for the three configurations under study. An increase in the  
5 potential was observed during the first minutes of operation. However, after that period,  
6 the system seemed to achieve a steady-state potential (mainly for carbon paper  
7 configuration), which led to a stable operation during the rest of the interval. This loss of  
8 efficiency has been reported in other works [9, 49] and can be assigned to several reasons.  
9 Many authors hold the idea that the deterioration of the system is related to either the  
10 higher swelling degree of the polymer membrane [50-53] or to the poisoning of the  
11 catalyst at higher concentrated alcohol solutions. Another option is the accumulation of  
12 reaction intermediates derived from the partial electro-oxidation of ethanol, which could  
13 be chemisorbed on the Pt active centers, causing the progressive increase in the potential  
14 [54]. In addition, ethanol crossover can play an important role for the stability of these  
15 systems, poisoning the cathode chamber [53-56]. Regarding the different configuration  
16 tested in this work, *a* and *c* show the best electrochemical behavior, reaching a constant  
17 cell potential close to 0.8 V for the applied current. The steady-state value was reached in  
18 a short period of time (10-20 min), which supposes very promising values compared to  
19 other ethanol electro-reforming studies, where the transition time was estimated in 3 h [9,  
20 11, 44]. Furthermore, the potential increase for the whole recorded range was very low  
21 for both configurations, approximately an increment of 0.02 V was registered after 2 h of  
22 experiment. This small decrease in the cell efficiency seems to be linked to the poisoning  
23 effect of adsorbed species on the catalyst layer instead of the swelling process, which  
24 would irreversibly destroy the MEA causing a noticeable increase in the potential.

1 Configuration *b* showed a different behaviour. The transition period until stabilization  
2 was significantly higher, requiring 1.8 V of cell potential to keep a constant applied  
3 current of 0.5 A, which is more than twice as much as it takes for carbon paper-based  
4 configurations to produce the same quantity of H<sub>2</sub>. Taking into account this loss of  
5 efficiency, a galvanostatic open circuit potential (OCV) regenerative test was carried out  
6 for configuration *b*. This essay was conducted under the same conditions as the previous  
7 experiment, but with application of OCV cycles of 30 s every 30 min. In Figure 6.b, both  
8 profiles (with and without regeneration) are compared. It can be observed that including  
9 OCV steps, the potential is reduced to the half, reaching a steady-state cell potential close  
10 to 1 V, which might be associated to the removal of intermediates under fluid circulation  
11 without the application of current. The corresponding energy consumption was calculated  
12 for all configurations, obtaining values close to 19.3 kW kgH<sub>2</sub><sup>-1</sup> for configurations *a* and  
13 *c*, while configuration *b* demanded 48 kW·kgH<sub>2</sub><sup>-1</sup> and 26.8 kW·kgH<sub>2</sub><sup>-1</sup> for the non-  
14 regenerative and regenerative tests, respectively. These results are very competitive  
15 compared with those energy requirements found in the literature at same operation  
16 conditions, which are around 27 kW·kgH<sub>2</sub><sup>-1</sup> [9].

17 Taken all into account, the MEA architecture of a PEM cell has proved to be a key variable  
18 with a considerably influence on the ethanol electro-reforming process. In this sense,  
19 configuration *c* (based on carbon paper as GDL and a catalyst layer directly supported on  
20 the membrane without high-temperature and pressure assembly step) showed the best  
21 electrochemical performance. This novel layout exhibited high electro-catalytic activity  
22 in continuous mode (without recycling) of operation, low energy requirements in terms  
23 of hydrogen production and a suitable organic product distribution, shifting the acetic  
24 acid generation to lower cell potential values.

25

## 1 4. Conclusions

2 In summary, the influence of different ways of MEA architectures on the ethanol electro-  
3 reforming process for the added-value product generation (organic compounds and  
4 hydrogen) has been studied. For that purpose, three different configurations were  
5 designed changing the GDL type (carbon paper or porous titanium), the assembly mode  
6 (high temperature-pressure assembly or non-assembly step) and the active phase  
7 deposition (over GDL/membrane). Carbon paper configurations (*a* and *c*) exhibited the  
8 best electrochemical performance, reaching high density current values (600 and 720  
9 mA·cm<sup>-2</sup>) in the linear sweep voltammetry tests (same order as those obtained for basic  
10 medium) and low potential profiles in the chronopotentiometry essays. Conversely,  
11 configuration *b* provided lower current density values (300 mA·cm<sup>-2</sup>) and a sharp increase  
12 in the potential for certain current steps, resulting in a low electrochemical activity,  
13 Even more, despite faradaic hydrogen production was obtained for all configuration, the  
14 energy requirements were much lower for carbon paper-based configurations compared  
15 to that based on a porous titanium architecture, which can be associated to a higher  
16 architecture resistance and mass transfer limitations offered by porous titanium.  
17 Regarding the value-added compounds production, the organic product distribution was  
18 found to vary with the different MEA architectures. Acetaldehyde and ethyl acetate  
19 production starts at potentials close to 0.5 V and 0.6 V for all configurations, while acetic  
20 acid production was higher for configuration *c*, shifting overpotential to a lower value  
21 (0.7 V) compared to the rest of configurations (close to 0.8 V). Finally, electrochemical  
22 impedance spectroscopy essays showed the lowest resistance values for carbon paper  
23 configurations, being slightly better for configuration *c*. In this sense, the catalytic layer  
24 deposited directly over the membrane proved to be more active in electro-catalytic terms,  
25 enhancing the mass transfer and the selectivity towards acetic acid.

## 1 Acknowledgments

2 We gratefully acknowledge the Spanish Ministry of Economy and Competitiveness  
3 (projects CTQ2016-75491-R) for the financial support.

## 4 References

- 5 [1] N. Lior, Sustainable energy development: The present (2009) situation and possible  
6 paths to the future, *Energy* 35 (2010) 3976-3994.10.1016/j.energy.2010.03.034
- 7 [2] C.Y. Park, T.H. Lee, S.E. Dorris, U. Balachandran, Hydrogen production from fossil  
8 and renewable sources using an oxygen transport membrane, *Int. J. Hydrogen Energ.* 35  
9 (2010) 4103-4110.10.1016/j.ijhydene.2010.02.025
- 10 [3] F. Barbir, Transition to renewable energy systems with hydrogen as an energy carrier,  
11 *Energy* 34 (2009) 308-312.10.1016/j.energy.2008.07.007
- 12 [4] F.I. Pires, P.G. Corradini, V.A. Paganin, E. Antolini, J. Perez, Effect of the degree of  
13 alloying of PtRu/C (1:1) catalysts on ethanol oxidation, *Ionics* 19 (2013) 1037-  
14 1045.10.1007/s11581-012-0822-9
- 15 [5] R.M. Altarawneh, P.G. Pickup, Product distributions and efficiencies for ethanol  
16 oxidation in a proton exchange membrane electrolysis cell, *J. Electrochem Soc.* 164  
17 (2017) F861-F865.10.1149/2.0051709jes
- 18 [6] R.M. Altarawneh, T.M. Brueckner, B. Chen, P.G. Pickup, Product distributions and  
19 efficiencies for ethanol oxidation at PtNi octahedra, *J. Power Sources* 400 (2018) 369-  
20 376.10.1016/j.jpowsour.2018.08.052
- 21 [7] Z. Hu, M. Wu, Z. Wei, S. Song, P.K. Shen, Pt-WC/C as a cathode electrocatalyst for  
22 hydrogen production by methanol electrolysis, *J. Power Sources* 166 (2007) 458-  
23 461.10.1016/j.jpowsour.2007.01.083
- 24 [8] C.R. Cloutier, D.P. Wilkinson, Electrolytic production of hydrogen from aqueous  
25 acidic methanol solutions, *Int. J. Hydrogen Energ.* 35 (2010) 3967-  
26 3984.10.1016/j.ijhydene.2010.02.005
- 27 [9] A.R. de la Osa, A.B. Calcerrada, J.L. Valverde, E.A. Baranova, A. de Lucas-  
28 Consuegra, Electrochemical reforming of alcohols on nanostructured platinum-tin  
29 catalyst-electrodes, *Appl. Catal. B-Environ* 179 (2015) 276-  
30 284.10.1016/j.apcatb.2015.05.026
- 31 [10] C. Lamy, T. Jaubert, S. Baranton, C. Coutanceau, Clean hydrogen generation  
32 through the electrocatalytic oxidation of ethanol in a Proton Exchange Membrane  
33 Electrolysis Cell (PEMEC): Effect of the nature and structure of the catalytic anode, *J.*  
34 *Power Sources* 245 (2014) 927-936.https://doi.org/10.1016/j.jpowsour.2013.07.028
- 35 [11] A. Caravaca, A. De Lucas-Consuegra, A.B. Calcerrada, J. Lobato, J.L. Valverde, F.  
36 Dorado, From biomass to pure hydrogen: Electrochemical reforming of bio-ethanol in a  
37 PEM electrolyser, *Appl. Catal. B-Environ* 134-135 (2013) 302-  
38 309.10.1016/j.apcatb.2013.01.033
- 39 [12] T. Take, K. Tsurutani, M. Umeda, Hydrogen production by methanol-water solution  
40 electrolysis, *J. Power Sources* 164 (2007) 9-16.10.1016/j.jpowsour.2006.10.011
- 41 [13] G. Sasikumar, A. Muthumeenal, S.S. Pethaiah, N. Nachiappan, R. Balaji, Aqueous  
42 methanol eletrolysis using proton conducting membrane for hydrogen production, *Int. J.*  
43 *Hydrogen Energ.* 33 (2008) 5905-5910.10.1016/j.ijhydene.2008.07.013
- 44 [14] J. Ivy, Summary of electrolytic hydrogen production: milestone completion report,  
45 National Renewable Energy Lab., Golden, CO (US), 2004.

- 1 [15] L. An, T.S. Zhao, Y.S. Li, Carbon-neutral sustainable energy technology: Direct  
2 ethanol fuel cells, *Renewable and Sustainable Energy Reviews* 50 (2015) 1462-  
3 1468.10.1016/j.rser.2015.05.074
- 4 [16] S.C. Zignani, V. Baglio, J.J. Linares, G. Monforte, E.R. Gonzalez, A.S. Aricò,  
5 Performance and selectivity of Pt xSn/C electro-catalysts for ethanol oxidation prepared  
6 by reduction with different formic acid concentrations, *Electrochim. Acta* 70 (2012) 255-  
7 265.10.1016/j.electacta.2012.03.055
- 8 [17] J. De Paula, D. Nascimento, J.J. Linares, Electrochemical reforming of glycerol in  
9 alkaline PBI-based PEM reactor for hydrogen production, *Chem. Engineer Trans.* 41  
10 (2014) 205-210.10.3303/cet1441035
- 11 [18] A.O. Neto, R.R. Dias, M.M. Tusi, M. Linardi, E.V. Spinacé, Electro-oxidation of  
12 methanol and ethanol using PtRu/C, PtSn/C and PtSnRu/C electrocatalysts prepared by  
13 an alcohol-reduction process, *J. Power Sources* 166 (2007) 87-  
14 91.10.1016/j.jpowsour.2006.12.088
- 15 [19] F. Vigier, C. Coutanceau, F. Hahn, E.M. Belgsir, C. Lamy, On the mechanism of  
16 ethanol electro-oxidation on Pt and PtSn catalysts: Electrochemical and in situ IR  
17 reflectance spectroscopy studies, *J. Electroanal. Chem.* 563 (2004) 81-  
18 89.10.1016/j.jelechem.2003.08.019
- 19 [20] L. Jiang, G. Sun, S. Sun, J. Liu, S. Tang, H. Li, B. Zhou, Q. Xin, Structure and  
20 chemical composition of supported Pt-Sn electrocatalysts for ethanol oxidation,  
21 *Electrochim. Acta* 50 (2005) 5384-5389.10.1016/j.electacta.2005.03.018
- 22 [21] S.W. Xie, S. Chen, Z.Q. Liu, C.W. Xu, Comparison of alcohol electrooxidation on  
23 Pt and Pd electrodes in alkaline medium, *Int. J. Electrochem. Sc.* 6 (2011) 882-888
- 24 [22] L. Xing, W. Shi, H. Su, Q. Xu, P.K. Das, B. Mao, K. Scott, Membrane electrode  
25 assemblies for PEM fuel cells: A review of functional graded design and optimization,  
26 *Energy* 177 (2019) 445-464.10.1016/j.energy.2019.04.084
- 27 [23] B. Thoben, A. Siebke, Influence of Different Gas Diffusion Layers on the Water  
28 Management of the PEFC Cathode, *J. New Mat. Electr. Syst.* 7 (2004) 13-20
- 29 [24] W. Li, R. Lin, Y. Yang, Investigation on the reaction area of PEMFC at different  
30 position in multiple catalyst layer, *Electrochim. Acta* 302 (2019) 241-  
31 248.https://doi.org/10.1016/j.electacta.2019.02.003
- 32 [25] A. Ozden, S. Shahgaldi, X. Li, F. Hamdullahpur, A review of gas diffusion layers  
33 for proton exchange membrane fuel cells—With a focus on characteristics,  
34 characterization techniques, materials and designs, *Prog. Energ. Combust.* 74 (2019) 50-  
35 102.https://doi.org/10.1016/j.pecs.2019.05.002
- 36 [26] A.T. Pham, T. Baba, T. Sugiyama, T. Shudo, Efficient hydrogen production from  
37 aqueous methanol in a PEM electrolyzer with porous metal flow field: Influence of PTFE  
38 treatment of the anode gas diffusion layer, *Int. J. Hydrogen Energ.* 38 (2013) 73-  
39 81.https://doi.org/10.1016/j.ijhydene.2012.10.036
- 40 [27] A.M. Dafalla, F. Jiang, Stresses and their impacts on proton exchange membrane  
41 fuel cells: A review, *Int. J. Hydrogen Energ.* 43 (2018) 2327-  
42 2348.https://doi.org/10.1016/j.ijhydene.2017.12.033
- 43 [28] E. Carcadea, M. Varlam, M. Ismail, D.B. Ingham, A. Marinoiu, M. Raceanu, C.  
44 Jianu, L. Patularu, D. Ion-Ebrasu, PEM fuel cell performance improvement through  
45 numerical optimization of the parameters of the porous layers, *Int. J. Hydrogen Energ.* 45  
46 (2020) 7968-7980.https://doi.org/10.1016/j.ijhydene.2019.08.219
- 47 [29] K. Jiao, B. Zhou, Innovative gas diffusion layers and their water removal  
48 characteristics in PEM fuel cell cathode, *J. Power Sources* 169 (2007) 296-  
49 314.10.1016/j.jpowsour.2007.03.042

- 1 [30] S. Park, J.W. Lee, B.N. Popov, A review of gas diffusion layer in PEM fuel cells:  
2 Materials and designs, *Int. J. Hydrogen Energ.* 37 (2012) 5850-  
3 5865.10.1016/j.ijhydene.2011.12.148
- 4 [31] V. Patel, L. Battrell, R. Anderson, N. Zhu, L. Zhang, Investigating effect of different  
5 gas diffusion layers on water droplet characteristics for proton exchange membrane  
6 (PEM) fuel cells, *Int. J. Hydrogen Energ.* 44 (2019) 18340-  
7 18350.10.1016/j.ijhydene.2019.05.111
- 8 [32] Q. Yan, H. Toghiani, H. Causey, Steady state and dynamic performance of proton  
9 exchange membrane fuel cells (PEMFCs) under various operating conditions and load  
10 changes, *J. Power Sources* 161 (2006) 492-502.10.1016/j.jpowsour.2006.03.077
- 11 [33] Z. Zhan, J. Xiao, Y. Zhang, M. Pan, R. Yuan, Gas diffusion through differently  
12 structured gas diffusion layers of PEM fuel cells, *Int. J. Hydrogen Energ.* 32 (2007) 4443-  
13 4451.10.1016/j.ijhydene.2007.03.041
- 14 [34] J. Ge, A. Higier, H. Liu, Effect of gas diffusion layer compression on PEM fuel cell  
15 performance, *J. Power Sources* 159 (2006) 922-927.10.1016/j.jpowsour.2005.11.069
- 16 [35] H. Görgün, M. Arcak, F. Barbir, A voltage-based observer design for membrane  
17 water content in PEM fuel cells, *P. Amer. Contr. Conf.* 2005, pp. 4796-4801.
- 18 [36] M. Stähler, A. Stähler, F. Scheepers, M. Carmo, W. Lehnert, D. Stolten, Impact of  
19 porous transport layer compression on hydrogen permeation in PEM water electrolysis,  
20 *Int. J. Hydrogen Energ.* 45 (2020) 4008-  
21 4014.https://doi.org/10.1016/j.ijhydene.2019.12.016
- 22 [37] Z. Wei, J. Sun, Y. Li, A.K. Datye, Y. Wang, Bimetallic catalysts for hydrogen  
23 generation, *Chem. Soc. Rev.* 41 (2012) 7994-8008.10.1039/c2cs35201j
- 24 [38] T. Corrales-Sánchez, J. Ampurdanés, A. Urakawa, MoS<sub>2</sub>-based materials as  
25 alternative cathode catalyst for PEM electrolysis, *Int. J. Hydrogen Energ.* 39 (2014)  
26 20837-20843.10.1016/j.ijhydene.2014.08.078
- 27 [39] H. Ju, S. Giddey, S.P.S. Badwal, R.J. Mulder, Electro-catalytic conversion of ethanol  
28 in solid electrolyte cells for distributed hydrogen generation, *Electrochim. Acta* 212  
29 (2016) 744-757.10.1016/j.electacta.2016.07.062
- 30 [40] G.S. Avcioglu, B. Ficicilar, I. Eroglu, Effect of PTFE nanoparticles in catalyst layer  
31 with high Pt loading on PEM fuel cell performance, *Int. J. Hydrogen Energ.* 41 (2016)  
32 10010-10020.10.1016/j.ijhydene.2016.03.048
- 33 [41] K. Leelaruji, M. Hunsom, Alcohol reduction-mediated preparation of a nano-scale  
34 Pt/C electrocatalyst for the oxygen reduction reaction in PEM fuel cells, *Renew. Energ.*  
35 35 (2010) 2422-2430.10.1016/j.renene.2010.02.019
- 36 [42] A. De Lucas-Consuegra, A.B. Calcerrada, A.R. De La Osa, J.L. Valverde,  
37 Electrochemical reforming of ethylene glycol. Influence of the operation parameters,  
38 simulation and its optimization, *Fuel Process. Technol.* 127 (2014) 13-  
39 19.10.1016/j.fuproc.2014.06.010
- 40 [43] S. Rousseau, C. Coutanceau, C. Lamy, J.M. Léger, Direct ethanol fuel cell (DEFC):  
41 Electrical performances and reaction products distribution under operating conditions  
42 with different platinum-based anodes, *J. Power Sources* 158 (2006) 18-  
43 24.10.1016/j.jpowsour.2005.08.027
- 44 [44] A. De Lucas-Consuegra, A.R. De La Osa, A.B. Calcerrada, J.J. Linares, D. Horwat,  
45 A novel sputtered Pd mesh architecture as an advanced electrocatalyst for highly efficient  
46 hydrogen production, *J. Power Sources* 321 (2016) 248-  
47 256.10.1016/j.jpowsour.2016.05.004
- 48 [45] H. Li, G. Sun, L. Cao, L. Jiang, Q. Xin, Comparison of different promotion effect of  
49 PtRu/C and PtSn/C electrocatalysts for ethanol electro-oxidation, *Electrochim. Acta* 52  
50 (2007) 6622-6629.10.1016/j.electacta.2007.04.056

- 1 [46] H. Wang, Z. Jusys, R.J. Behm, Ethanol electro-oxidation on carbon-supported Pt,  
2 PtRu and Pt3Sn catalysts: A quantitative DEMS study, *J. Power Sources* 154 (2006) 351-  
3 359.10.1016/j.jpowsour.2005.10.034
- 4 [47] A. Caravaca, F.M. Sapountzi, A. De Lucas-Consuegra, C. Molina-Mora, F. Dorado,  
5 J.L. Valverde, Electrochemical reforming of ethanol-water solutions for pure H<sub>2</sub>  
6 production in a PEM electrolysis cell, *Int. J. Hydrogen Energ.* 37 (2012) 9504-  
7 9513.10.1016/j.ijhydene.2012.03.062
- 8 [48] Y.X. Chen, A. Lavacchi, H.A. Miller, M. Bevilacqua, J. Filippi, M. Innocenti, A.  
9 Marchionni, W. Oberhauser, L. Wang, F. Vizza, Nanotechnology makes biomass  
10 electrolysis more energy efficient than water electrolysis, *Nat. Commun.* 5  
11 (2014).10.1038/ncomms5036
- 12 [49] J. Lobato, P. Cañizares, M.A. Rodrigo, J.J. Linares, B. Sánchez-Rivera, Testing  
13 different catalysts for a vapor-fed PBI-based direct ethanol fuel cell, *Proceedings of the*  
14 *7th International Conference on Fuel Cell Science, Engineering, and Technology 2009,*  
15 *2009*, pp. 23-28.
- 16 [50] A.M. Affoune, A. Yamada, M. Umeda, Conductivity and surface morphology of  
17 Nafion membrane in water and alcohol environments, *J. Power Sources* 148 (2005) 9-  
18 17.10.1016/j.jpowsour.2005.01.039
- 19 [51] D. Rivin, C.E. Kendrick, P.W. Gibson, N.S. Schneider, Solubility and transport  
20 behavior of water and alcohols in Nafion™, *Polymer* 42 (2001) 623-635.10.1016/s0032-  
21 3861(00)00350-5
- 22 [52] J.A. Elliott, S. Hanna, A.M.S. Elliott, G.E. Cooley, The swelling behaviour of  
23 perfluorinated ionomer membranes in ethanol/water mixtures, *Polymer* 42 (2001) 2251-  
24 2253.10.1016/s0032-3861(00)00538-3
- 25 [53] S. Song, G. Wang, W. Zhou, X. Zhao, G. Sun, Q. Xin, S. Kontou, P. Tsiakaras, The  
26 effect of the MEA preparation procedure on both ethanol crossover and DEFC  
27 performance, *J. Power Sources* 140 (2005) 103-110.10.1016/j.jpowsour.2004.08.011
- 28 [54] S. Song, P. Tsiakaras, Recent progress in direct ethanol proton exchange membrane  
29 fuel cells (DE-PEMFCs), *Appl. Catal. B-Environ* 63 (2006) 187-  
30 193.10.1016/j.apcatb.2005.09.018
- 31 [55] V. Alzate, K. Fatih, H. Wang, Effect of operating parameters and anode diffusion  
32 layer on the direct ethanol fuel cell performance, *J. Power Sources* 196 (2011) 10625-  
33 10631.10.1016/j.jpowsour.2011.08.080
- 34 [56] K. Taneda, Y. Yamazaki, Study of direct type ethanol fuel cells. Analysis of anode  
35 products and effect of acetaldehyde, *Electrochim. Acta* 52 (2006) 1627-  
36 1631.10.1016/j.electacta.2006.03.093

37

38

39

40

41

42

43

44

1 **Figure captions**

2 Figure 1. Scheme of MEA configurations.

3 Figure 2. Linear sweep voltammetry tests for each configuration at 0-1.4 V potential  
4 range. 80°C, 1 atm and 20 mV·s<sup>-1</sup> scan rate.

5 Figure 3. Electrochemical impedance spectroscopy essays. a) Nyquist diagram for  
6 Configuration *a* at 0.5-0.9 V potential range, b) Comparative for each configuration at  
7 0.5 V.

8 Figure 4. Stepped chronopotentiometry for each configuration between 0.2-0.8 A.

9 Figure 5. Liquid products distribution for each configuration from Figure 4. a)  
10 Configuration *a*, b) Configuration *b*, c) Configuration *c*. 0.2-0.8 A.

11 Figure 6. Mild-term stability at 0.5 A of applied current. a) Potential profiles for each  
12 configuration, b) comparative between standard and OCV mild-term test for  
13 Configuration *b*.

14

15

16

17

18

19

20

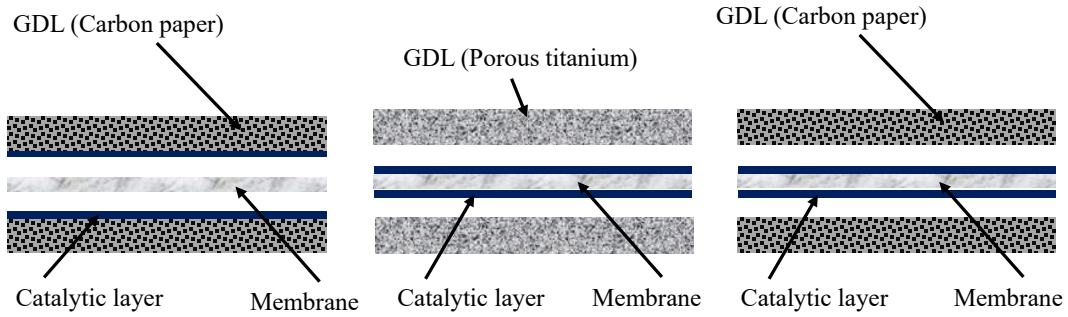
21

22

23

24

25



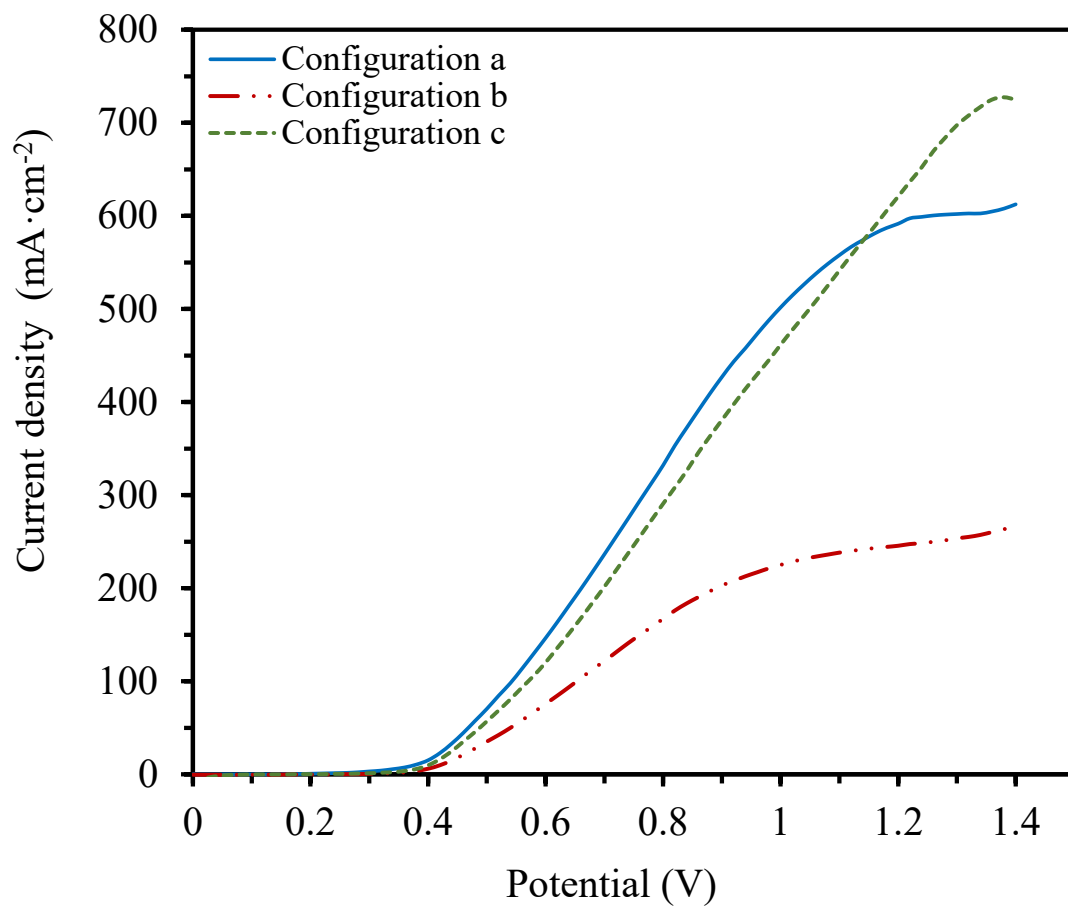
**a)** Catalytic layer deposited over the carbon paper. GDL: Carbon paper.

**b)** Catalytic layer deposited over the membrane. GDL: Porous Titanium.

**c)** Catalytic layer deposited over the membrane. GDL: Carbon paper.

Figure 1.

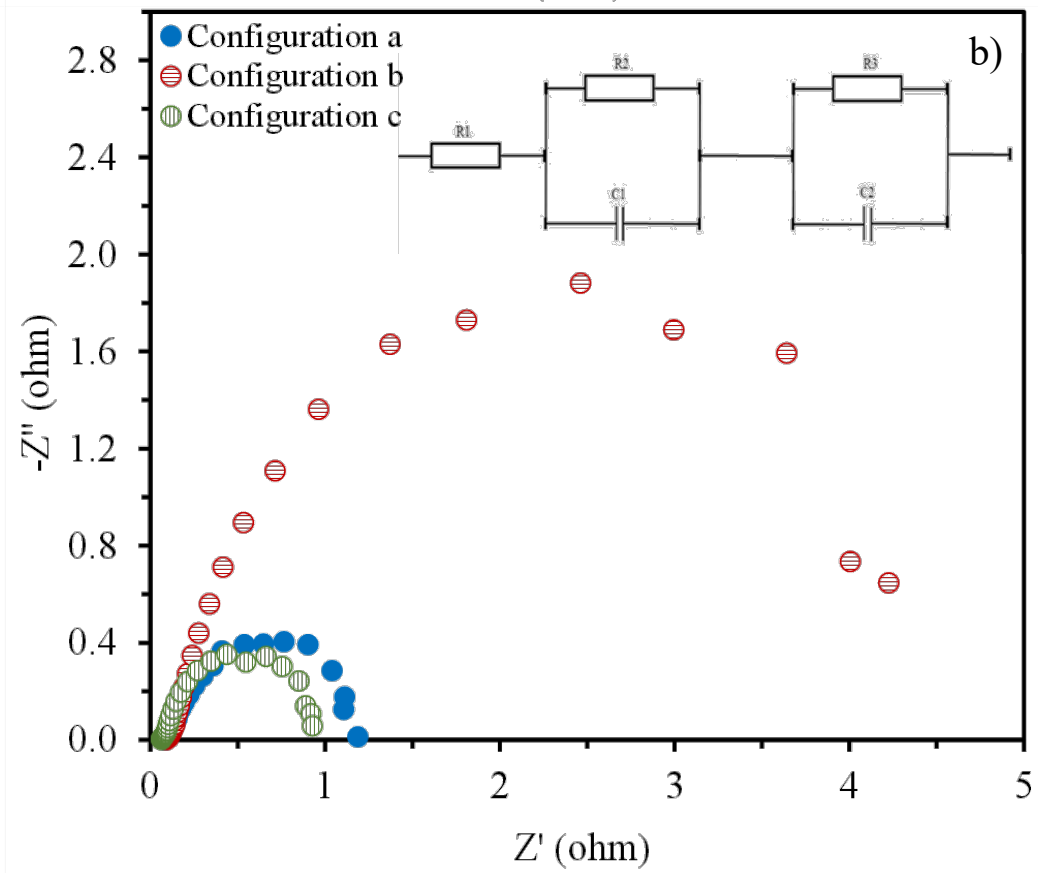
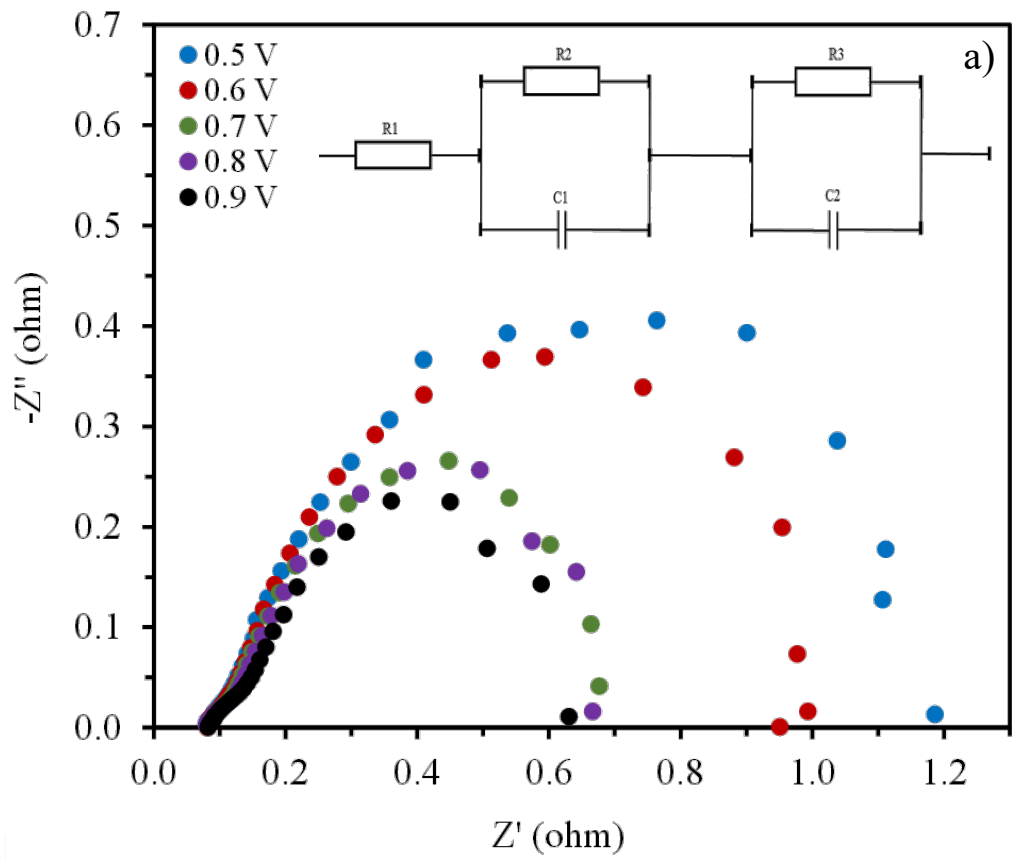
- 2
- 3
- 4
- 5
- 6
- 7
- 8
- 9
- 10
- 11
- 12
- 13
- 14
- 15
- 16
- 17
- 18
- 19



2

Figure 2.

3



1  
2

Figure 3.

1  
2  
3

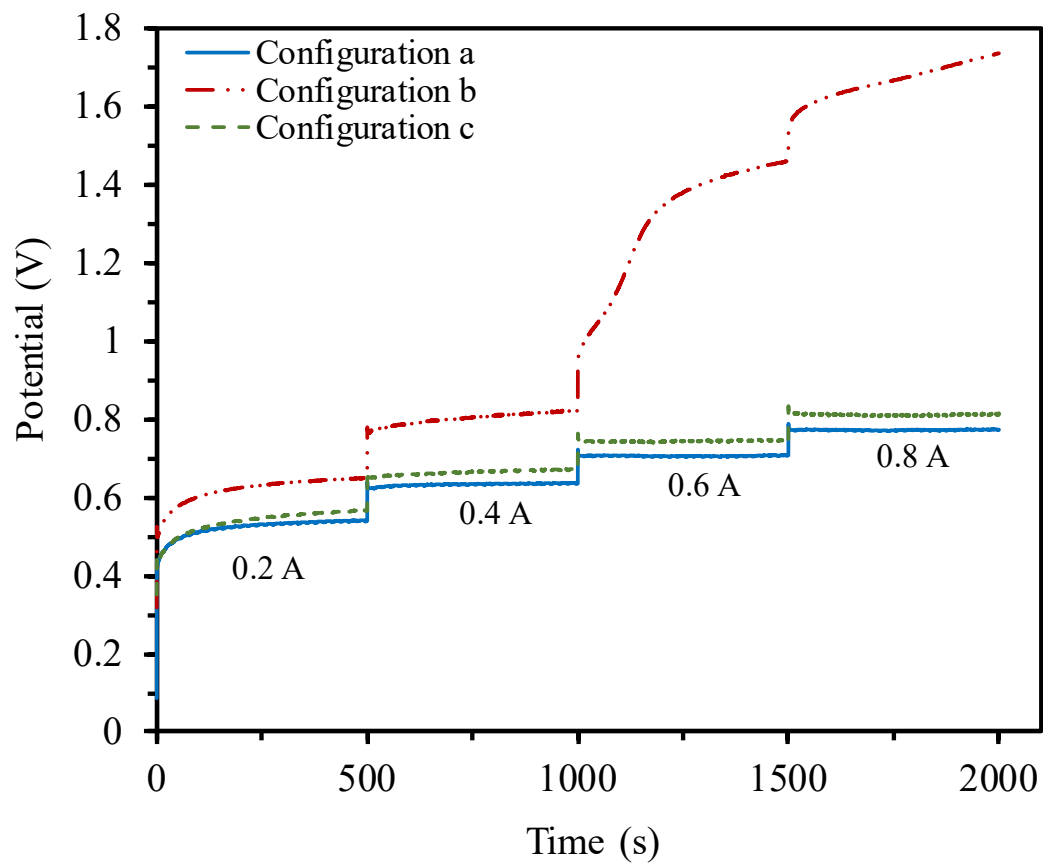


Figure 4.

5  
6  
7  
8  
9  
10  
11  
12  
13  
14  
15  
16

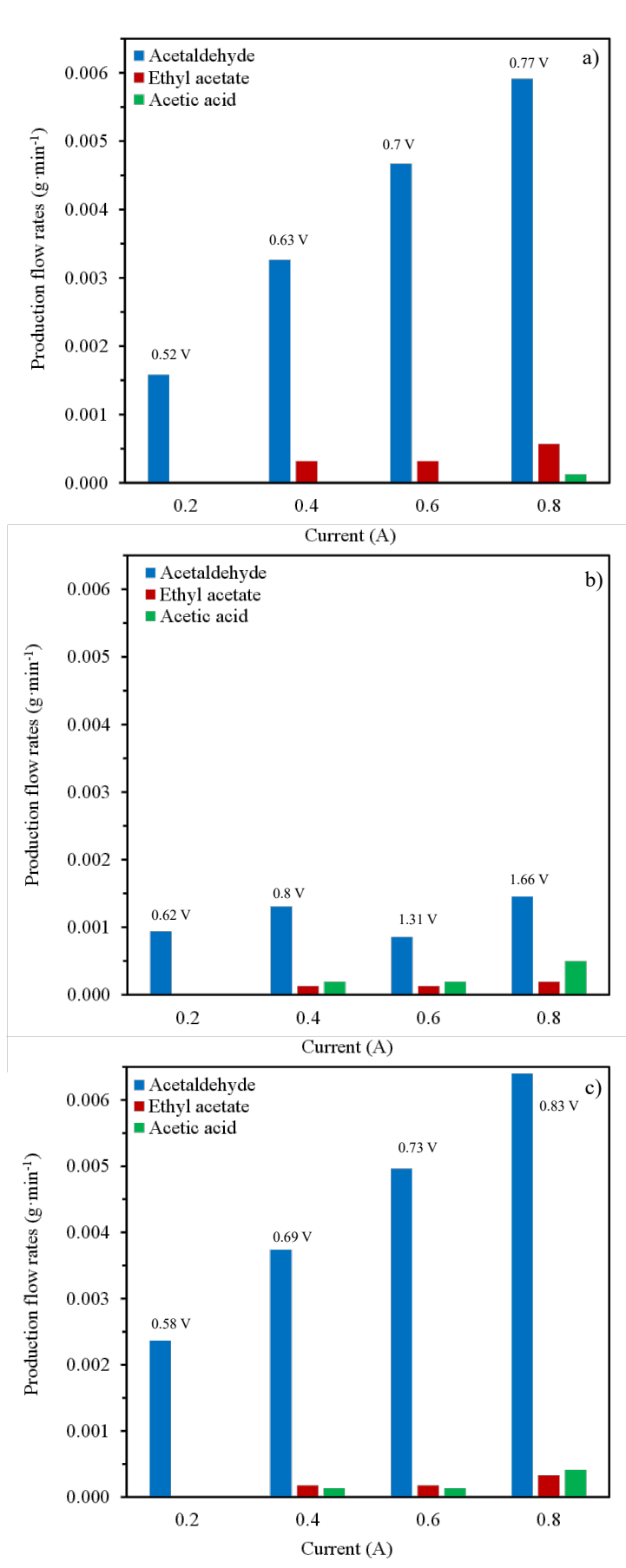
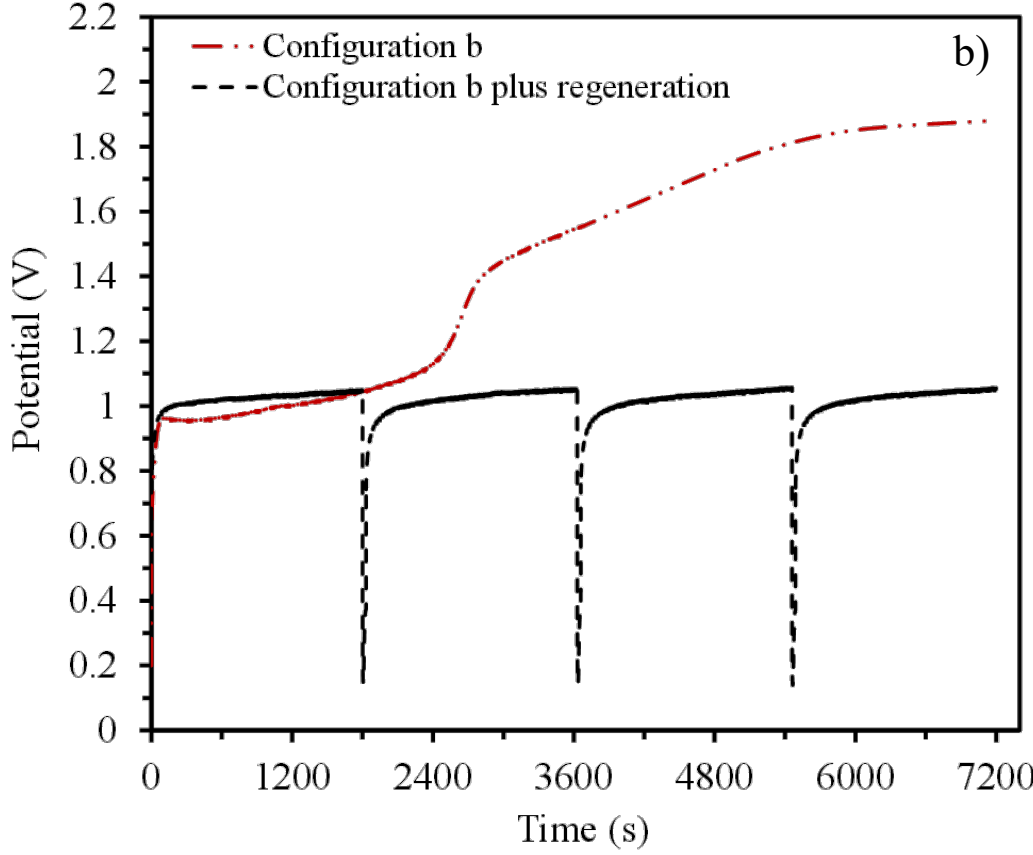
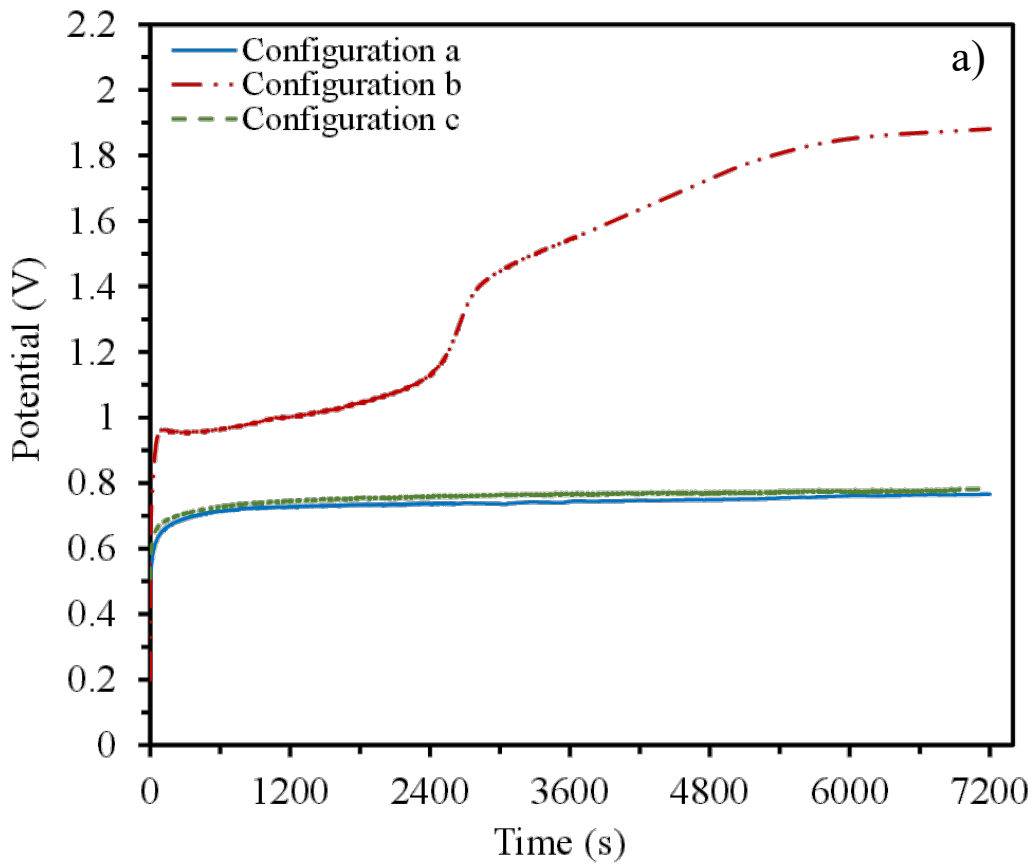


Figure 5.



1  
2

Figure 6.

1 **Table captions**

2 Table 1. Electrochemical impedance spectroscopy fitted parameters for the potential  
3 range of study. Configuration *a*.

4 Table 2. Electrochemical impedance spectroscopy fitted parameters for all configurations  
5 at 0.5 V of applied potential.

6 Table 3. Energetic requirements comparison for all configurations at different levels of  
7 current.

8

9

10

11

12

13

14

15

16

17

18

19

20

21

22

23

24

25

26

27

1  
2  
3  
4  
5  
6  
7  
8  
9  
10  
11  
12  
13  
14  
15  
16  
17  
18  
19  
20  
21  
22  
23  
24  
25  
26  
27  
28  
29  
30

Table 1.

Applied potential (V)					
Components	0.5	0.6	0.7	0.8	0.9
<i>R1</i> (ohm)	0.094	0.092	0.089	0.089	0.092
<i>R2</i> (ohm)	0.813	0.741	0.515	0.507	0.441
<i>R3</i> (ohm)	0.099	0.078	0.056	0.056	0.062
<i>C1</i> (F)	0.131	0.131	0.111	0.098	0.089
<i>C2</i> (F)	0.053	0.046	0.023	0.015	0.013

1  
2  
3  
4  
5  
6  
7  
8  
9  
10  
11  
12  
13  
14  
15  
16  
17  
18  
19  
20  
21  
22  
23  
24  
25  
26  
27  
28  
29  
30

Table 2.

Components	Configuration <i>a</i>	Configuration <i>b</i>	Configuration <i>c</i>
<i>R1</i> (ohm)	0.094	0.111	0.088
<i>R2</i> (ohm)	0.813	3.410	0.773
<i>R3</i> (ohm)	0.099	0.134	0.053
<i>C1</i> (F)	0.131	0.051	0.042
<i>C2</i> (F)	0.053	0.045	0.024

1

2

3

4

Table. 3

Current (A)	$V_m$ (V)			Power (W)			Total energy consumption (kWh·kgH <sub>2</sub> <sup>-1</sup> )		
	Configuration								
	<i>a</i>	<i>b</i>	<i>c</i>	<i>a</i>	<i>b</i>	<i>c</i>	<i>a</i>	<i>b</i>	<i>c</i>
0.2	0.52	0.62	0.58	0.10	0.12	0.12	14.0	16.6	14.4
0.4	0.63	0.80	0.69	0.25	0.32	0.28	16.9	21.5	17.7
0.6	0.7	1.31	0.73	0.42	0.78	0.46	18.9	35.2	19.9
0.8	0.77	1.66	0.83	0.62	1.33	0.66	20.7	44.6	21.7

5

6

7

8